

Fig. 3.1. Crystal structure of sapphire: $\alpha\text{-Al}_2\text{O}_3$ (aluminum oxide). The shaded atoms make up a unit cell of the structure. The aluminum atom inside the dashed hexagonal prism experiences an almost cubic field symmetry from the oxygen atoms on the prism^[3.1].

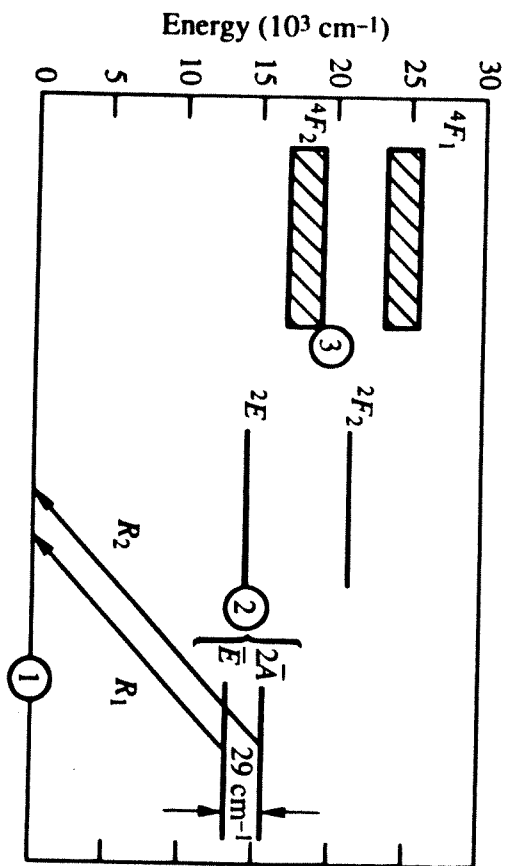


Fig. 3.2. Schematic energy level diagram for ruby - Cr³⁺ ions in sapphire^[3.2].

Fig. 3.3. Absorption coefficient and absorption cross-section as a function of wavelength for pink ruby. These absorption spectra are slightly different depending on whether the incident polarized light being absorbed is linearly polarized with its electric vector parallel, or perpendicular, to the c symmetry axis of the crystal^[3.3].

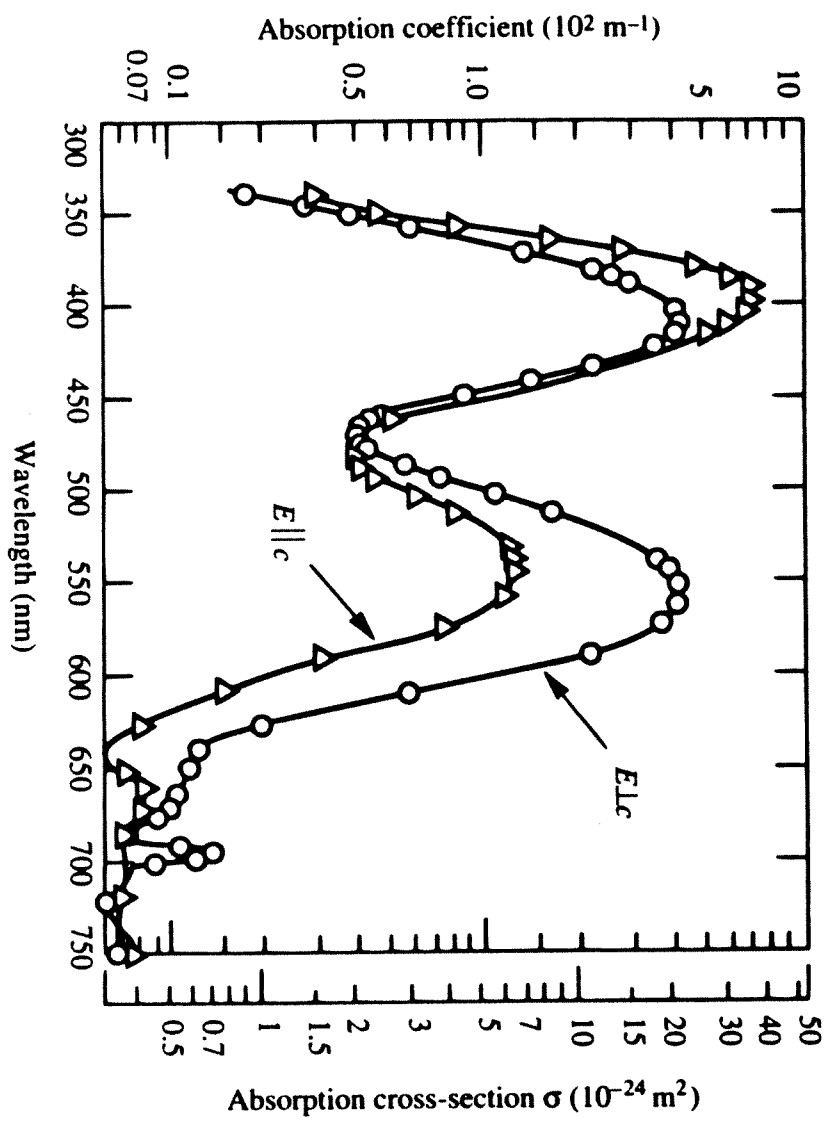
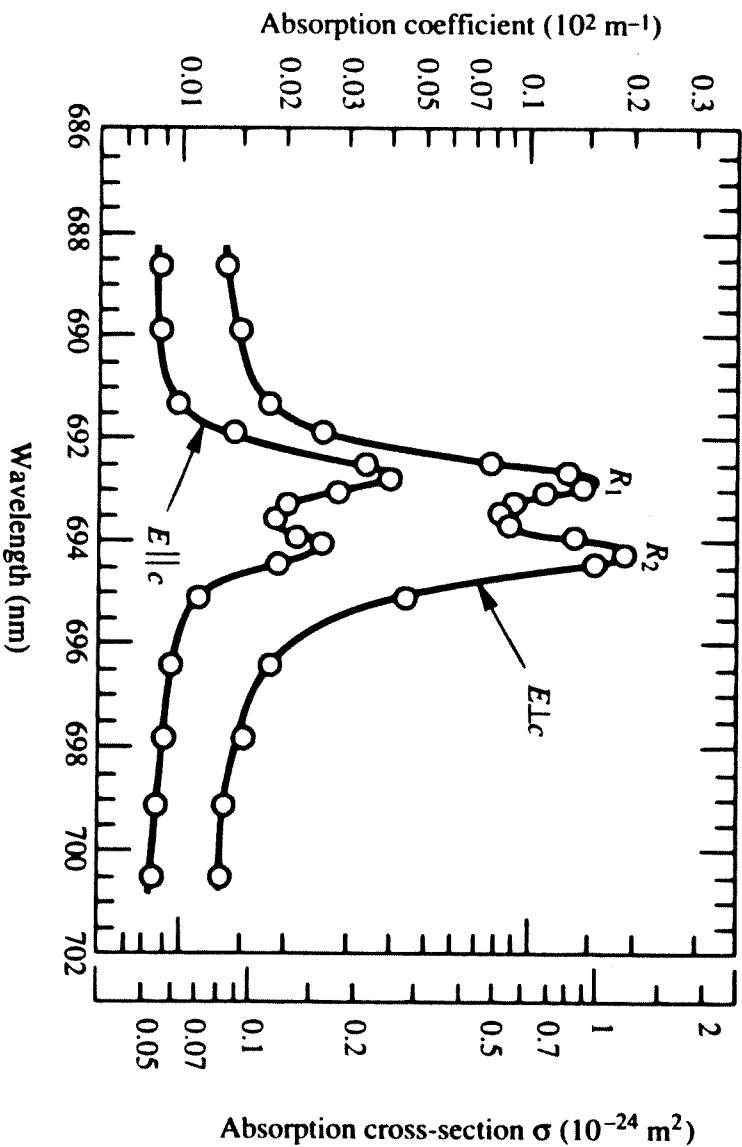


Fig. 3.4. Detailed absorption spectrum of pink ruby in the 686-702 nm region showing the absorption peaks corresponding to the R_1 and R_2 components of the ruby laser transition [3.3].



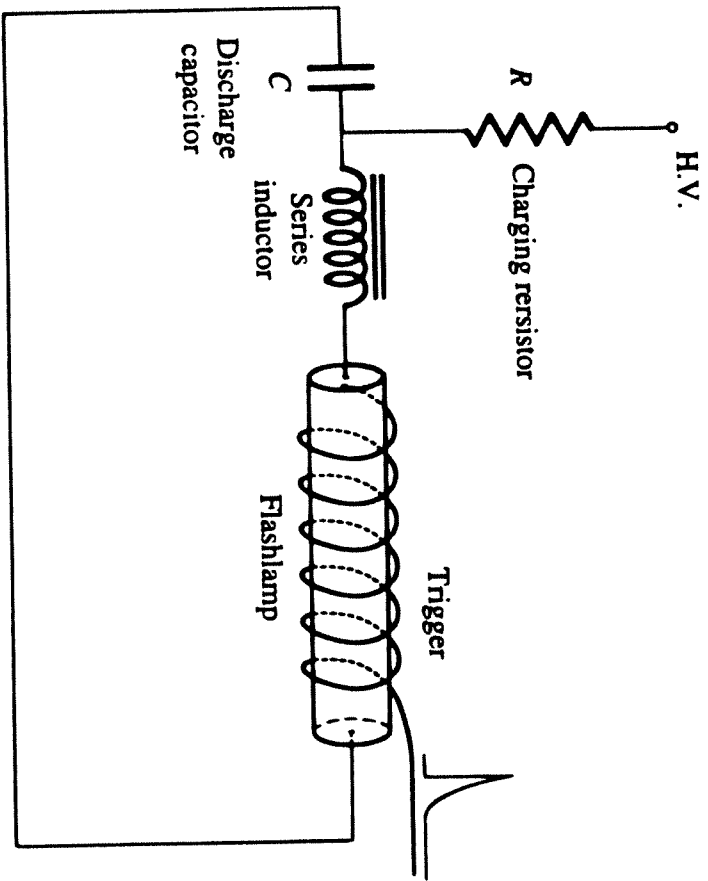
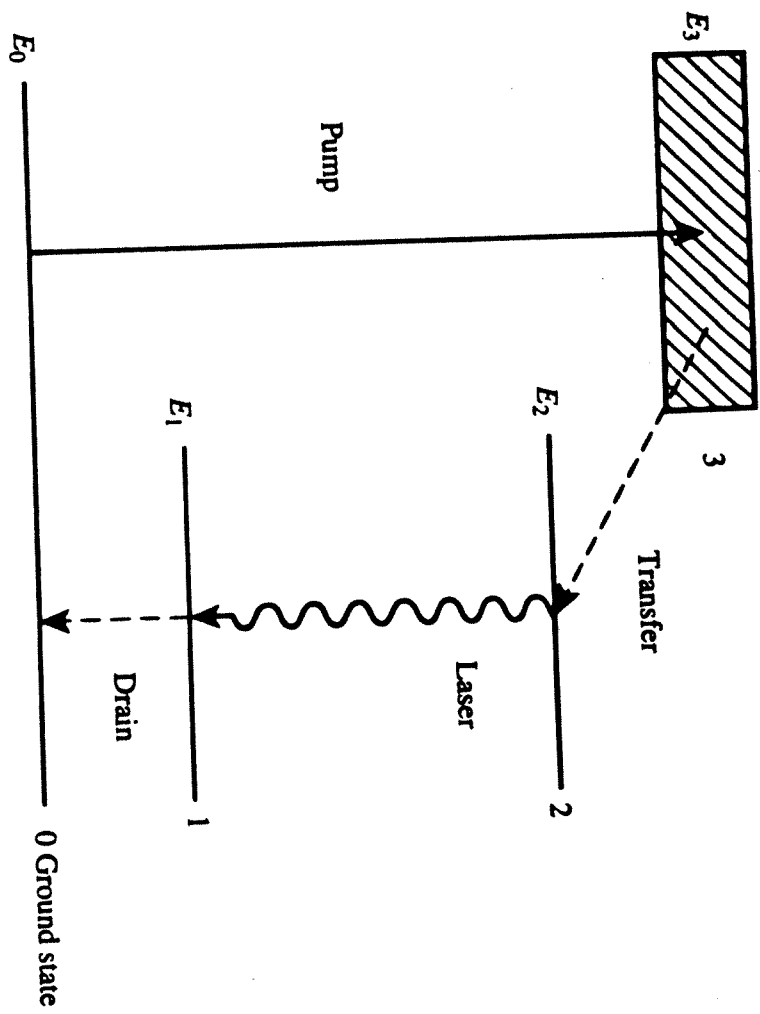


Fig. 3.5. Simple electrical circuit for driving a flashlamp.

Fig 3.6. Schematic energy level diagram of three- and four-level lasers.



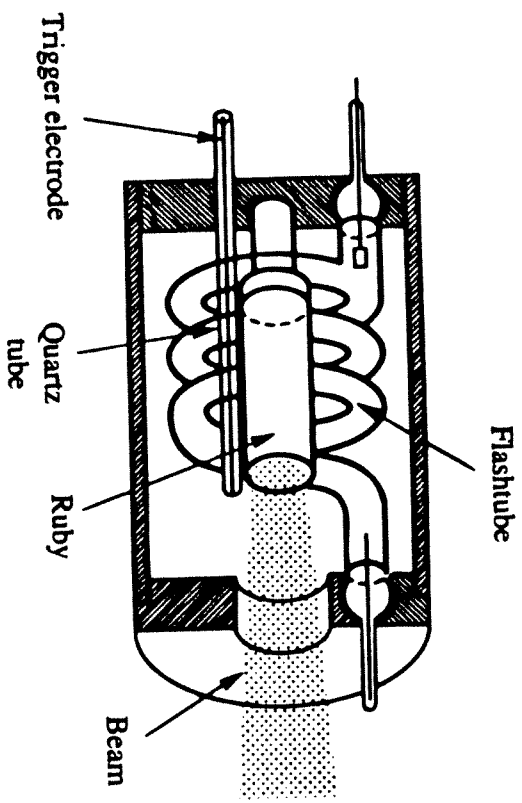


Fig. 3.7. Schematic arrangement of Maiman's original ruby laser.

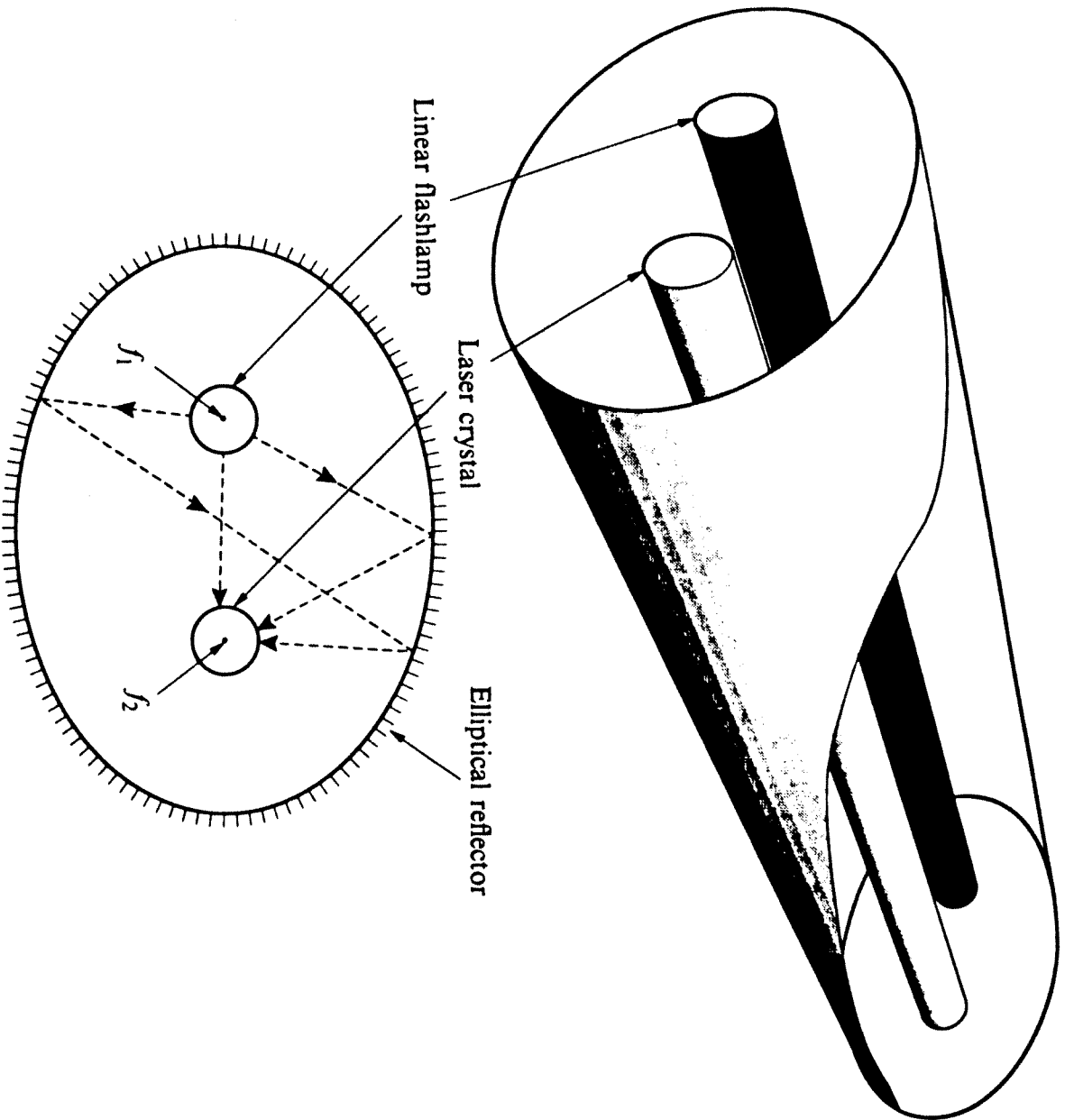
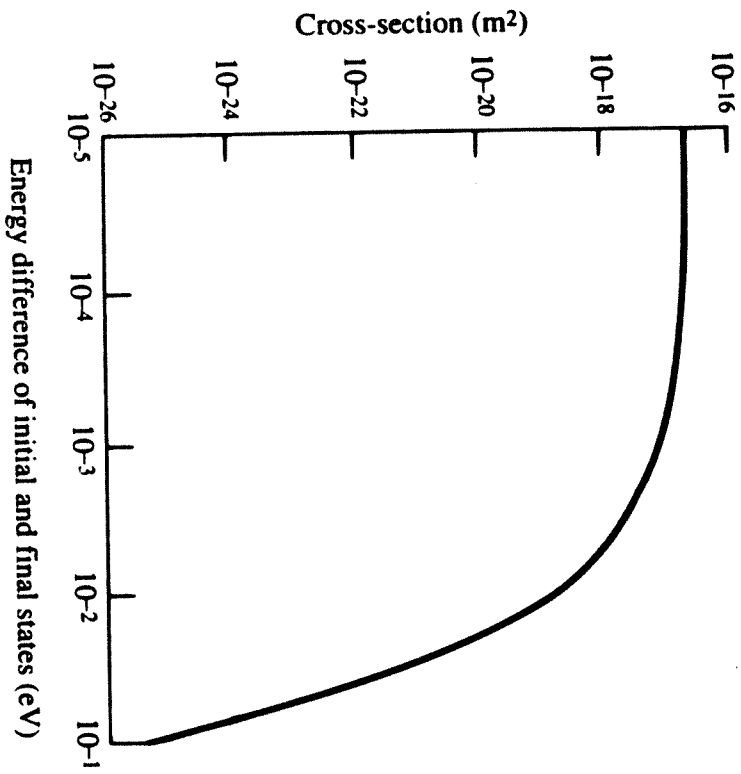


Fig. 3.8. Elliptical reflector arrangement for optical pumping of a laser crystal by a linear flashlamp.

Fig. 3.9. Calculated variation of energy transfer cross-section for a collision between two atomic species as a function of the energy discrepancy ΔE_x [3.3]. The probability of excitation transfer is linearly dependent on the cross-section.



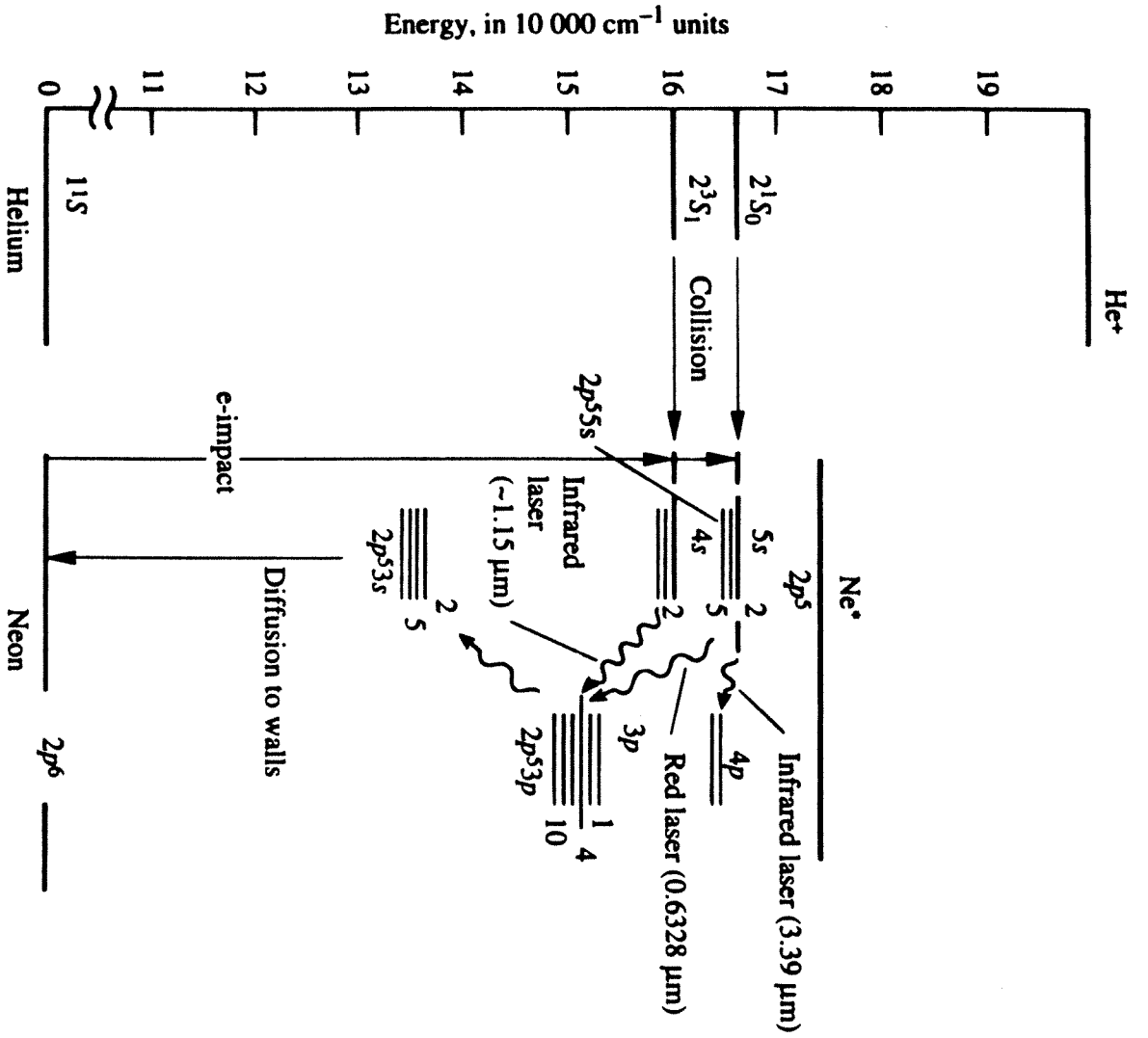
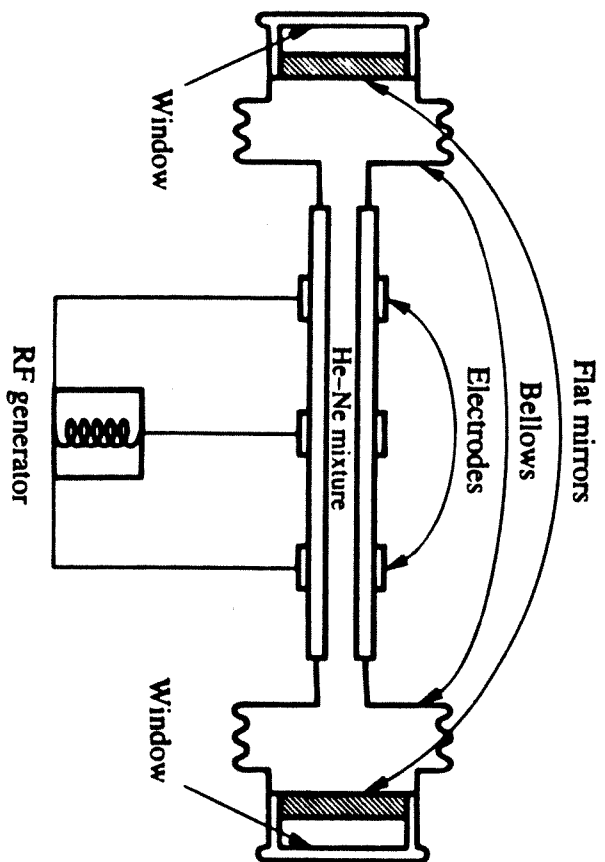


Fig. 3.10. Energy level diagram for the helium-neon laser.

Fig. 3.11. Schematic arrangement of the first gas laser.



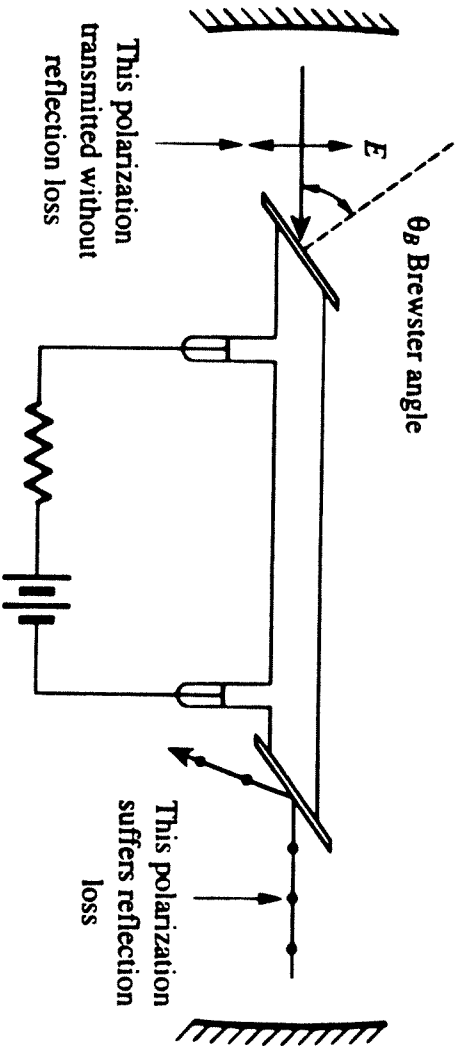


Fig. 3.12. Typical schematic design of a modern gas laser.